PCCP

PAPER

View Article Online
View Journal | View Issue

Cite this: *Phys. Chem. Chem. Phys.*, 2014, **16**, 1150

Proton transfer and hydrogen bonding in the organic solid state: a combined XRD/XPS/ssNMR study of 17 organic acid–base complexes†

Joanna S. Stevens,*[a] Stephen J. Byard,[b] Colin C. Seaton,[a] Ghazala Sadiq,[a] Roger J. Davey[a] and Sven L. M. Schroeder*[ac]

Received 14th September 2013,
Accepted 5th November 2013

DOI: 10.1039/c3cp53907e

www.rsc.org/pccp

The properties of nitrogen centres acting either as hydrogen-bond or Brønsted acceptors in solid molecular acid–base complexes have been probed by N 1s X-ray photoelectron spectroscopy (XPS) as well as ^{15}N solid-state nuclear magnetic resonance (ssNMR) spectroscopy and are interpreted with reference to local crystallographic structure information provided by X-ray diffraction (XRD). We have previously shown that the strong chemical shift of the N 1s binding energy associated with the protonation of nitrogen centres unequivocally distinguishes protonated (salt) from hydrogen-bonded (co-crystal) nitrogen species. This result is further supported by significant ssNMR shifts to low frequency, which occur with proton transfer from the acid to the base component. Generally, only minor chemical shifts occur upon co-crystal formation, unless a strong hydrogen bond is formed. CASTEP density functional theory (DFT) calculations of ^{15}N ssNMR isotropic chemical shifts correlate well with the experimental data, confirming that computational predictions of H-bond strengths and associated ssNMR chemical shifts allow the identification of salt and co-crystal structures (NMR crystallography). The excellent agreement between the conclusions drawn by XPS and the combined CASTEP/ssNMR investigations opens up a reliable avenue for local structure characterization in molecular systems even in the absence of crystal structure information, for example for non-crystalline or amorphous matter. The range of 17 different systems investigated in this study demonstrates the generic nature of this approach, which will be applicable to many other molecular materials in organic, physical, and materials chemistry.

Introduction

The crystallization of solid state acid–base donor–acceptor systems with more than one component is a commonly used route to tailor the physical and chemical properties of solid organic products and their formulations. For example, during the development of active pharmaceutical ingredients (APIs), the physicochemical properties of the pure API may be unsuitable for a chosen drug delivery route. Combining with a Brønsted donor or acceptor can result in intermolecular bonding, either by forming an ionic (salt) or hydrogen-bonded (co-crystal[1–3]) complex with superior properties,[1–4] which may include solubility,[5] bioavailability,[5,6] chemical and physical stability,[7,8] hygroscopicity,[9] and mechanical properties.[10,11]

Single crystal X-ray diffraction (XRD) is most commonly used for determining whether proton transfer or hydrogen bonding takes place between acid and base components,[3,5,12–18] often in conjunction with an analysis of structural indicators such as bond angles and bond lengths.[3,12,16,19] However, the unequivocal determination of hydrogen positions is not always straightforward, particularly with systems exhibiting proton disorder, temperature-dependent migration, or other unusual behaviour.[18] Analysis by XRD is also constrained by a requirement for suitable single crystals, which may not be available when solid-state preparation techniques such as milling are used to form materials with more than one component.[20,21] Where single crystal XRD fails other commonly available laboratory techniques such as vibrational spectroscopies can sometimes provide the required information.[12,13] Often, however, the determination of hydrogen and proton positions has to rely on more advanced techniques such as neutron diffraction,[12,18,19]as demonstrated for, *e.g.*, urea/phosphoric acid,[17,22,23] 4,4′-bipyridyl/benzene-1,2,4,5-tetracarboxylic acid,[24] 4-methylpyridine/pentachlorophenol,[25] and benzoic acid.[26,27]

[a] *School of Chemical Engineering and Analytical Science, The University of Manchester, Oxford Road, Manchester, M13 9PL, UK. E-mail: joanna.stevens@manchester.ac.uk, s.schroeder@manchester.ac.uk*
[b] *Covance Laboratories, Willowburn Avenue, Alnwick, Northumberland, NE66 2JH, UK*
[c] *School of Chemistry, The University of Manchester, Oxford Road, Manchester, M13 9PL, UK*

† CCDC 960081 and 960082. For crystallographic data in CIF or other electronic format see DOI: 10.1039/c3cp53907e

Over the last decade, solid-state NMR (ssNMR) methods combined with computational chemical shift analysis[5,28,29] have been added to the inventory of techniques for the characterisation of hydrogen bonding and Brønsted interactions in the organic solid state. Studies have shown that H-bonding and proton transfer in two-component systems can be distinguished using ^{15}N ssNMR,[5,21,29–32] as for example shown for co-crystals and salts of a cancer-treatment API[5] and for theophylline (1,3-dimethyl-7*H*-purine-2,6-dione) systems.[21,28,30] Density functional theory (DFT) can be applied to correlate ^{15}N ssNMR parameters with crystal structures. For example, calculations for the co-crystal form of a pharmaceutical API correctly predicted chemical shifts (to low frequency) relative to the free base on formation of strong H-bonds, in agreement with experimental data.[5] Similarly, comparison of predicted ^{15}N chemical shift values for complexes of dabco (1,4-diazabicyclo[2.2.2]-octane) and dicarboxylic acids with experimental data confirmed Brønsted and H-bonding interactions in these systems.[29]

Recently, we reported that X-ray photoelectron spectroscopy (XPS) also reliably detects proton transfer: a strong positive N 1s binding energy shift occurs due to protonation and identifies the formation of a salt.[21,28,30,33] The information of this chemical shift analysis is conceptually very similar to that used in the ssNMR approach,[28] opening up an avenue to mutual validation of results obtained with either technique. The principle of a large N 1s shift with protonation was applied to identify the nature of *meta*-aminobenzoic acid polymorphs (non-ionic *vs.* zwitterionic),[34] and an O 1s shift to higher binding energy was also observed for an oxygen proton acceptor with formation of a H-bond on moving from the gas to condensed phase.[35] Very importantly, long-range order is not a pre-requisite for the application of XPS and ssNMR; both techniques are also applicable to systems for which single crystal XRD would be unfeasible, for example when a suitable single crystal cannot be obtained, or when non-crystalline or amorphous samples are analysed.[36]

The feasibility of a combined ssNMR/XPS approach to local structure characterization in the organic solid state was introduced for theophylline co-crystal/salt systems,[28] but to explore it more systematically we report here the examination of the nature of the intermolecular interactions between components of 17 acid–base complexes (Table 1 and Fig. 1), comparing XPS results with experimental and calculated ^{15}N ssNMR data. As in our previous XPS study,[33] we incorporate several development API substances alongside a range of non-development acid–base complexes including theophylline, aminobenzoic, and isonicotinamide base components with different acid co-formers and thus differing acid strength.

These systems cover a wide range of pK_a differences (ΔpK_a), from −3.9 to +17.7, between the acceptor and donor functional groups, which will allow us to examine correlations between ΔpK_a values and the chemical shifts observable by XPS and ssNMR in a systematic manner. Of the 17 complexes, 6 (4 salts, 2 co-crystals) are within the range $0 < \Delta pK_a < 3$ (Table 1), for which it is generally unpredictable whether H-bonding or proton transfer takes place.[12,37]

Table 1 ΔpK_a values for the seventeen complexes (base/acid), where $\Delta pK_a = pK_a$ (base) $- pK_a$ (acid) based on pK_a values.[4,12,38–40] For complexes involving two acids, the pK_a of the more basic compound (with more basic substituent) is taken as pK_a (base)

	Salt or co-crystal	ΔpK_a
4-Aminobenzoic acid/ 4-hydroxy-3-nitrobenzoic acid	C	−3.9
Isonicotinamide/4-hydroxy-3-nitrobenzoic acid	C	−3.0
Theophylline/glutaric acid	C	−2.6
Theophylline/citric acid	C	−1.4
Theophylline/malonic acid	C	−1.1
4-Aminobenzoic acid/3,5-dinitrobenzoic acid	C	−0.3
Theophylline/maleic acid	C	−0.2
Theophylline/oxalic acid	C	0.3
Fumaric acid co-crystal **1c**	C	0.3
Isonicotinamide/2,4,6-trihydroxybenzoic acid	S	1.8
Theophylline/5-sulfosalicylic acid dihydrate	S	2.3
Theophylline/5-sulfosalicylic acid monohydrate	S	2.3
3,5-Diaminobenzoic acid/3,5-dinitrobenzoic acid	S	2.5
Difumarate salt **2**	S	7.2, 4.6
Di-HCl salt **1s**	S	11.3, 3.3
HCl salt **3**	S	15.4
HCl salt **4**	S	17.7

Experimental

Starting materials

All non-development starting materials were obtained with >99% purity (Sigma-Aldrich, UK); co-crystal or salt formation was verified by comparison of X-ray powder diffraction (XRPD) patterns to known structures[7,21,28,41–43] or XPS/ssNMR/XRD for new complexes. The five development complexes were used as supplied (Sanofi-Aventis, Alnwick) and comprise the dihydrochloride salt (**1s**) and fumaric acid co-crystal (**1c**) of an API **1**, the difumarate salt **2**, and the hydrochloride salts **3** and **4**.

Preparation of salts and co-crystals

The non-development co-crystals and salts were prepared by solid-state-grinding (milling) or solution crystallization. Milling was performed with a Retsch MM200 mixer mill at a rate of 30 Hz, using two 5 mL stainless steel jars, each containing one 7 mm-diameter stainless steel ball. The complexes were prepared as follows:

(i) 1 : 1 Theophyllinium salicylic-5-sulfonate dihydrate salt was prepared by both milling and solution crystallization as described previously.[28]

(ii) 1 : 1 Theophyllinium salicylic-5-sulfonate monohydrate salt was prepared by both milling and solution crystallization as described previously.[30]

(iii) 2 : 1 Theophylline/oxalic acid co-crystal was prepared by both milling and solution crystallization as described previously.[30]

(iv) 1 : 1 Theophylline/maleic acid co-crystal. Anhydrous theophylline (2.023 g, 11.23 mmol) and maleic acid (1.303 g, 1 equiv.) were dissolved in 35 mL of a 6 : 1 chloroform : methanol solvent mixture under reflux (53 °C). The solution was removed from heat and allowed to cool to ambient temperature while stirring. The resulting precipitate was removed by filtration under vacuum to give co-crystals with an excess of anhydrous theophylline. The filtrate was then allowed to stand overnight,

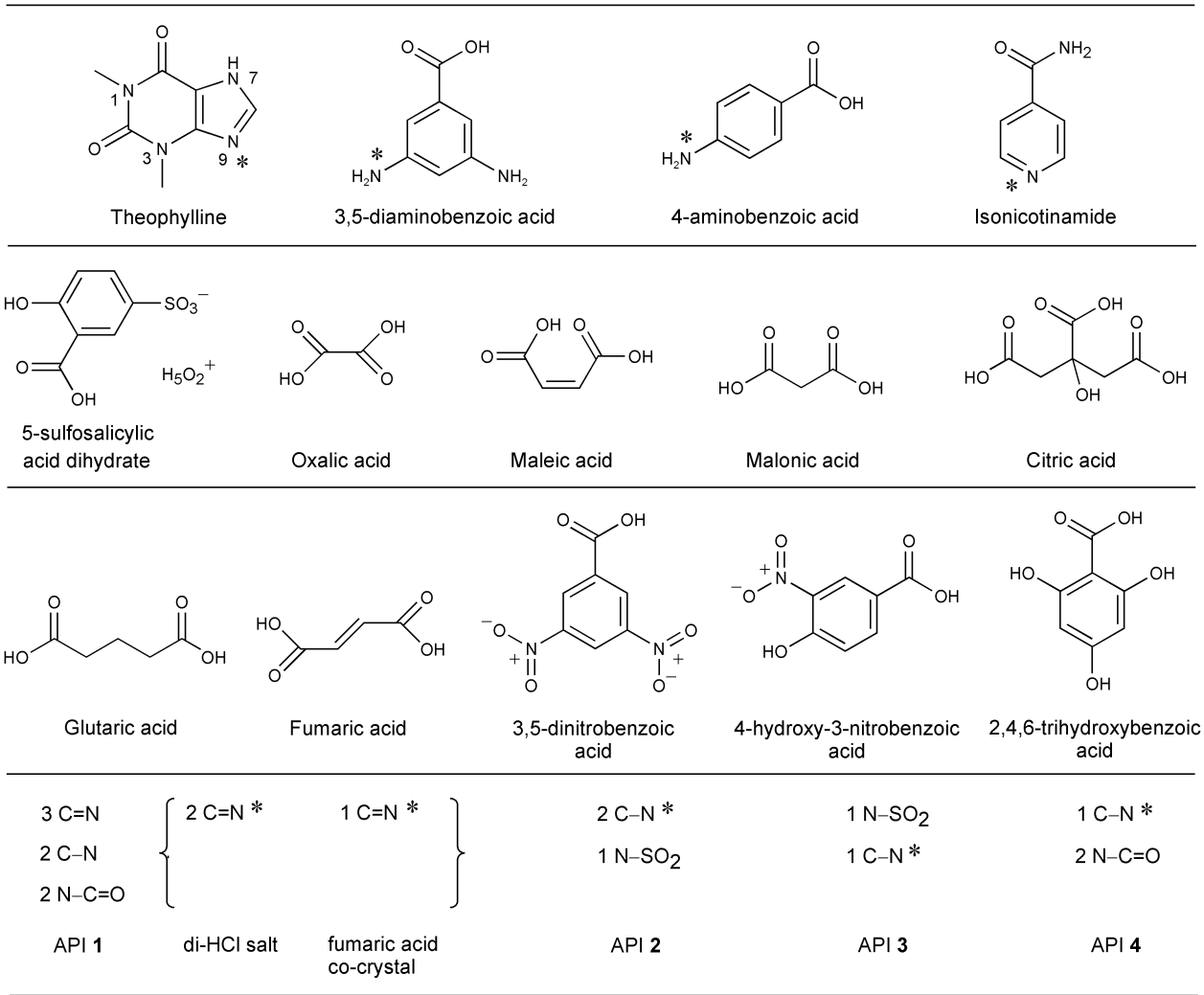

Fig. 1 Chemical structures of the individual components (the nitrogen moieties are listed for the development drug substances). The asterisks (*) indicate the nitrogen atoms sensitive to protonation (Brønsted donation) or intermolecular H-bonding in this study.

affording the physically pure 1 : 1 co-crystal, which was isolated by filtration under vacuum. The 1 : 1 co-crystal was also formed by milling theophylline (109.99 mg, 0.61 mmol) and maleic acid (70.80 mg, 1 eq.) for 20 minutes.

(v) 1 : 1 Theophylline/malonic acid co-crystal. Milling anhydrous theophylline (111.70 mg, 0.62 mmol) and malonic acid (64.52 mg, 1 eq.) for 20 minutes formed the 1 : 1 co-crystal. Anhydrous theophylline (0.5873 g, 3.26 mmol) and malonic acid (0.3392 g, 1.0 equiv.) were also dissolved in 40 mL chloroform and 2 mL methanol under reflux (55 °C). The solution was removed from heat and seeded with ~45 mg of co-crystal formed by milling. The solution was allowed to evaporate until ~15 mL remained, and then filtered under vacuum to give the 1 : 1 co-crystal.

(vi) 1 : 1 Theophylline/citric acid co-crystal was prepared by milling as described previously.[21]

(vii) 1 : 1 Theophylline/glutaric acid co-crystal. Milling anhydrous theophylline (93.7 mg, 0.52 mmol) and glutaric acid (68.7 mg, 1 eq.) for 60 minutes formed the 1 : 1 co-crystal, which was physically pure as determined by X-ray powder diffraction. Theophylline (0.4972 g, 2.76 mmol) and glutaric acid (0.3646 g, 1 equiv.) were also dissolved in 35 mL chloroform under reflux (59 °C). The solution was removed from heat and seeded with ~35 mg of co-crystal formed by milling. The solution was allowed to evaporate until ~20 mL volume remained, and the precipitate (present at the surface) was filtered under vacuum to give the 1 : 1 co-crystal.

(viii) 1 : 1 3,5-Diaminobenzoic acid/3,5-dinitrobenzoic acid salt. 3,5-Dinitrobenzoic acid (0.4176 g, 2 mmol) and 3,5-diaminobenzoic acid (0.3148 g, 2 mmol) were dissolved in 95% ethanol (25 mL), heated to ensure complete dissolution and left to slowly cool. Dark brown needle crystals were obtained.

(ix) 1 : 1 4-Aminobenzoic acid/3,5-dinitrobenzoic acid co-crystal. 4-Aminobenzoic acid (0.3477 g, 2.5 mmol) and 3,5-dinitrobenzoic acid (0.5596 g, 2.6 mmol) were dissolved in methanol (20 mL). The resulting yellow solution was left to slowly evaporate and yellow crystals were obtained.

(x) 1 : 1 4-Aminobenzoic acid/4-hydroxy-3-nitrobenzoic acid co-crystal. 4-Aminobenzoic acid (0.1372 g, 1 mmol) and

4-hydroxy-3-nitrobenzoic acid (0.1359 g, 0.7 mmol) were mixed in methanol (1 mL) and heated to 50 °C, and subsequently cooled to 10 °C at a rate of 0.5 °C min^{-1} using an Avantium Crystal16.[44] Orange-yellow block crystals were obtained.

(xi) 1 : 1 Isonicotinamide/2,4,6-trihydroxybenzoic acid salt. Isonicotinamide (0.0619 g, 5 mmol) and 2,4,6-trihydroxybenzoic acid monohydrate (0.1227 g, 7 mmol) were dissolved in methanol (7.5 mL). The sample was heated to ensure complete dissolution and left to cool to room temperature. On slow evaporation, light brown, blocky crystals were produced.

(xii) 1 : 1 Isonicotinamide/4-hydroxy-3-nitrobenzoic acid co-crystal. Isonicotinamide (0.666 g, 6 mmol) and 4-hydroxy 3-nitrobenzoic acid (0.9309 g, 5 mmol) were dissolved in hot methanol (35 mL). Upon cooling the solution was left to slowly evaporate until yellow crystals were obtained.

X-ray diffraction (XRD)

Powder XRD patterns were collected using a Rigaku Miniflex instrument utilizing Cu K_α radiation (λ = 1.5406 Å), operating over 5–40° 2θ at 1.5° min^{-1} with a 0.03° step, 30 kV voltage, and 15 mA current. Typically 5 mg of the sample was placed on a small sample attachment and smoothed to achieve a level surface.

Single crystal XRD data were collected at 100 K using an Oxford Diffraction X-Calibur 2 diffractometer utilizing Mo K_α radiation (λ = 0.71073 Å) and an Oxford CryoSystems Cryostream Controller 700. Data reduction, cell refinement, and multi-scan absorption corrections were carried out using the program CrysAlis RED (Oxford Diffraction Ltd., version 1.171.32.24, 2008). The isonicotinamide/4-hydroxybenzoic acid co-crystal structure was solved with SHELXS-97 and refined on F^2 against all reflections with SHELXL-97.[45] The isonicotinamide/2,4,6-trihydroxybenzoic acid salt structure was solved with SIR92[46] and refined on F^2 against all reflections using SHELXL-97.[45] All non-hydrogen atoms were refined by direct methods anisotropically; hydrogen atoms were located in difference Fourier maps and refined isotropically, or placed in geometric positions and refined as riding atoms. CCDC 960081 and 960082.†

X-ray photoelectron spectroscopy (XPS)

XP spectra were recorded using a Kratos Axis Ultra instrument employing a monochromatic Al K_α source (1486.69 eV), a hemispherical analyser with a hybrid (electrostatic and magnetic) lens system, charge neutralization by filament-generated, magnetically channeled low-energy electrons, and a delay line detector (DLD). Samples were fixed using double-sided tape. Experiments were performed while operating the X-ray source with a power of 180 W (15 kV and 12 mA), with the pressure below 10^{-8} mbar during analysis. The instrument was operated in CAE (constant analysis energy) mode, with a pass energy of 20 eV for high resolution scans of the photoemission from individual core levels, with a calibrated intensity/energy response and transmission function.[36] High resolution spectra were measured within the spectral range of interest (*ca.* ±20 eV around the core level emission peaks) with 0.1 eV steps and 300–500 ms dwell time per data point. Repeats were carried out to check for radiation damage.

Analysis of the data was carried out using Casa XPS software.[47] A linear background was used in all curve-fitting (minimizing χ^2)[47,48] along with a GL(30) lineshape (70% Gaussian, 30% Lorentzian using the Gaussian/Lorentzian product form).[47] For the remainder of this paper, when referring to spectral contributions of specific atoms in the molecular structure in the text, the atom of interest will be indicated by being underlined. Samples naturally containing aliphatic C–C environments were referenced to adventitious hydrocarbon contamination at 285 eV.[48] Samples without C–C environments were referenced to the lowest E_B photoemission; those containing citric acid were referenced to C–COOH (β-COOH) at 285.2 eV[49] due to the absence of a clear hydrocarbon shoulder; samples containing 5-sulfosalicylic acid were referenced to C=C at 284.8 eV.[50] Individual chemical environments/functional groups often exhibit similar ranges of binding energy values where the bonding or electronegativity is similar, thus where peaks arising from photoemission from different chemical environments occurred at the same position or within ±0.1 eV, a single peak was used to represent both environments for clarity and ease of discussion. Repeatability of the peak positions was within 0.1 eV.

Solid-state nuclear magnetic resonance (ssNMR)

Solid-state ^{15}N cross-polarisation magic angle spinning (CP-MAS) data were acquired using a Bruker DRX500 spectrometer operating at 50.69 MHz, equipped with a standard bore magnet and a 4 mm CP-MAS probe. The magic angle adjustment was optimized using KBr and field homogeneity optimized using adamantane. Data were collected using a spectral width of 30.3 kHz, 3072 complex data points, and an acquisition time of 50.8 ms. The relaxation delay and contact time were optimized for each individual sample. Sample rotation rates of 5.0–8.0 kHz were employed and typically greater than 2048 transients acquired. ^1H decoupling was achieved using a TPPM-15 sequence (86.2 kHz). Chemical shifts (δ_N) were referenced indirectly with respect to nitromethane, a standard recommended by IUPAC,[51,52] *via* the high frequency signal of a traceable standard of ammonium nitrate (δ_N = −5.1 ppm). Chemical shifts for the theophylline and API **1** salts and co-crystals are compared with the values for the free base forms by the change in chemical shift ($\Delta\delta = \delta_{complex} - \delta_{free\ base}$).

Isotropic chemical shift differences[53] were calculated using the CASTEP density functional theory (DFT) code,[54–56] which employs the gauge including projector augmented wave (GIPAW) algorithm. The generalised gradient approximation (GGA) PBE functional was used with core-valence interactions described by ultrasoft pseudo-potentials generated on-the-fly. Integrals over the Brillouin zone were completed using a Monkhorst–Pack grid with a reciprocal space *k*-point spacing of 0.04 $Å^{-1}$. A cut-off energy of 610 eV was defined for kinetic energy of planewaves used to provide a basis for wavefunctions. For each crystal structure, full geometry optimization was performed using an energy cut-off of 300 eV and a *k*-point spacing of 0.05 $Å^{-1}$, with fixed lattice parameters. Calculations were performed using Materials Studio version 4.4, as provided by Accelrys.[57] CASTEP DFT chemical shielding values (σ) were obtained for the nitrogen atoms of the theophylline, 4-aminobenzoic acid,

3,5-diaminobenzoic acid, and isonicotinamide complexes using the previously reported[7,21,28,41–43] and new isonicotinamide co-crystal/salt crystal structures as input. Shielding values for the co-crystal and salts are compared with chemical shifts by plotting calculated chemical shieldings (σ) *versus* experimental chemical shifts (δ_N). A plot of calculated chemical shieldings (σ) *versus* experimental chemical shifts (δ_N) for all of the CASTEP data gives a linear correlation with $y = -0.9525x - 153.61$ (R^2 = 0.9893). Predicted chemical shift differences use the free base as a reference [$\Delta\delta_{calc} = -(\sigma_{complex} - \sigma_{free\ base})$].

Results and discussion

XPS

The four nitrogen environments (Fig. 1) in the theophylline complexes result in two X-ray photoemission peak components.[21,28,30] The peak arising from the C–N/N–C=O nitrogens occurs at 401.0 ± 0.1 eV for both the co-crystal and salt forms (Fig. 2, Table 2). In the five theophylline co-crystals, the C=N photoemission occurs at 399.6 ± 0.1 eV. However, for the two theophylline salts, this second photoemission peak is at 401.9 eV (Fig. 2b, Table 2), with protonation (C=NH$^+$) shifting the C=N peak by +2.3 eV.[28,30]

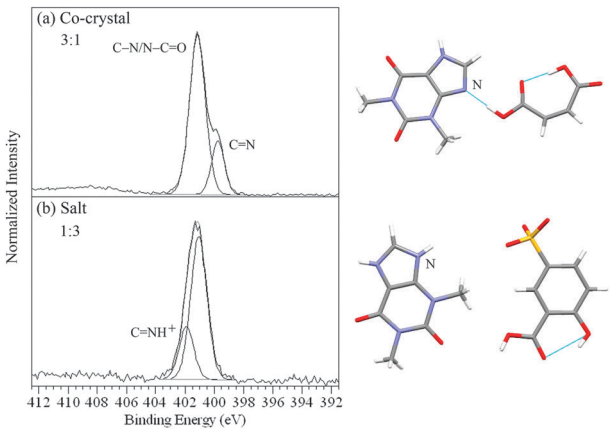

Fig. 2 N 1s XPS spectra of (a) the theophylline/maleic acid co-crystal and (b) the theophylline/5-sulfosalicylic acid dihydrate salt (C=NH$^+$, SO_3^-)[28] showing the ratios for types of nitrogen and the corresponding intermolecular H-bonding/protonation from the single crystal XRD structures[7,28] with the nitrogen sensitive to H-bonding/protonation marked.

The 4-aminobenzoic and 3,5-diaminobenzoic complexes all have at least one primary amine nitrogen C–NH_2 on the base component and a nitro group NO_2 on the acid component (Fig. 1 and 3). For the 4-aminobenzoic acid/3,5-dinitrobenzoic acid and 4-aminobenzoic acid/4-hydroxy-3-nitrobenzoic acid co-crystals (heterodimer bonding) this gives rise to two peaks at 399.5 ± 0.1 eV and 406.3 eV, from C–NH_2 and NO_2 respectively (Fig. 3a and b, Table 2).[40] When a salt is formed, as in the case of the 3,5-diaminobenzoic acid/3,5-dinitrobenzoic acid complex, one of the two amine nitrogens of 3,5-diaminobenzoic acid is protonated (C–NH_3^+), shifting its peak position to a higher binding energy of 401.9 eV, a shift of +2.4 eV (Fig. 3c, Table 2).[40]

There are three different types of nitrogen atom in isonicotinamide/4-hydroxy-3-nitrobenzoic acid – pyridine C=N and amide N–C=O of isonicotinamide and nitro NO_2 of the acid molecule (Fig. 1). The nitrogen 1s XPS (Fig. 4a) shows two maxima, with the high binding energy peak at 406.3 eV arising from the NO_2 photoemsission, while the lower energy peak can be fit with two components at 399.6 and 400.1 eV representing the C=N and amide N–C=O nitrogen functionalities respectively. With 2,4,6-trihydroxybenzoic acid, there are no nitrogens in the acid molecule (no NO_2 photoemission), leaving just the C=N and N–C=O from isonicotinamide. Aside from the isonicotinamide N–C=O peak at 400.1 eV, the C=N peak is shifted by 2.0 eV compared to that of isonicotinamide/4-hydroxy-3-nitrobenzoic acid and is observed at 401.6 eV, representing the change in chemical state from pyridine C=N to the pyridinium nitrogen C=NH$^+$ and evidence of salt formation (Fig. 4b, Table 2). Subsequent acquisition of the single crystal structure confirms the XPS-assignment of isonicotinamide/4-hydroxy-3-nitrobenzoic

Table 2 XPS N 1s peak assignments and positions

	Binding energy/eV							
Complex (base/acid)	N–SO_2	C–N	C=N	C=N···HO	N–C=O	C–NH^+	C=NH^+	NO_2
Theophylline/5-sulfosalicylic acid dihydrate salt		401.0			401.0		401.9	
Theophylline/5-sulfosalicylic acid monohydrate salt		401.0			401.0		401.9	
Theophylline/oxalic acid co-crystal		401.0	399.6		401.0			
Theophylline/maleic acid co-crystal		401.1	399.7		401.1			
Theophylline/malonic acid co-crystal		401.1	399.7		401.1			
Theophylline/citric acid co-crystal		400.9	399.5		400.9			
Theophylline/glutaric acid co-crystal		401.0	399.5		401.0			
4-Aminobenzoic acid/3,5-dinitrobenzoic acid co-crystal		399.4						406.3
4-Aminobenzoic acid/4-hydroxy-3-nitrobenzoic acid co-crystal		399.6						406.3
3,5-Diaminobenzoic acid/3,5-dinitrobenzoic acid salt		399.5				401.9		406.3
Isonicotinamide/4-hydroxy-3-nitrobenzoic acid co-crystal			399.6		400.1			406.3
Isonicotinamide/2,4,6-trihydroxybenzoic acid salt					400.1		401.6	
Di-HCl salt **1s**		399.1	399.1		400.3		401.2	
Fumaric acid co-crystal **1c**		399.2	399.2	399.8	400.6			
Difumarate salt **2**	399.5					401.7		
HCl salt **3**	399.6					401.7		
HCl salt **4**					399.9	401.5		

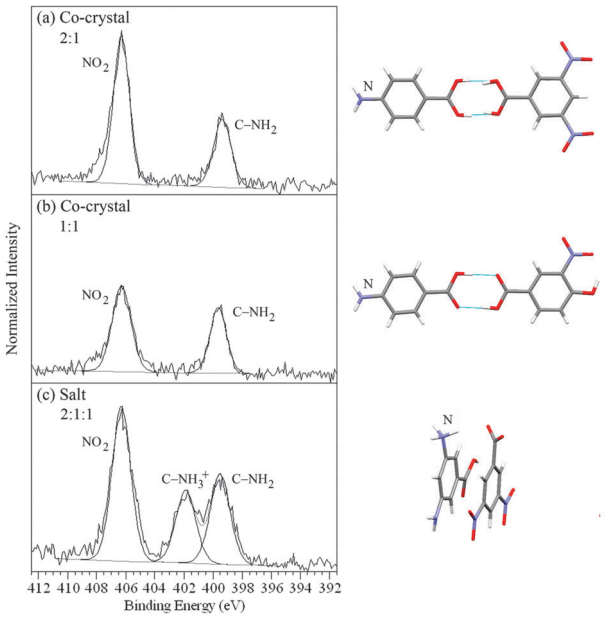

Fig. 3 N 1s XPS spectra of (a) the 4-aminobenzoic acid/3,5-dinitrobenzoic acid co-crystal, (b) the 4-aminobenzoic acid/4-hydroxy-3-nitrobenzoic acid co-crystal, and (c) the 3,5-diaminobenzoic acid/3,5-dinitrobenzoic acid salt (NH_3^+, COO^-), with the corresponding intermolecular H-bonding/protonation from the single crystal XRD structures.[42,43]

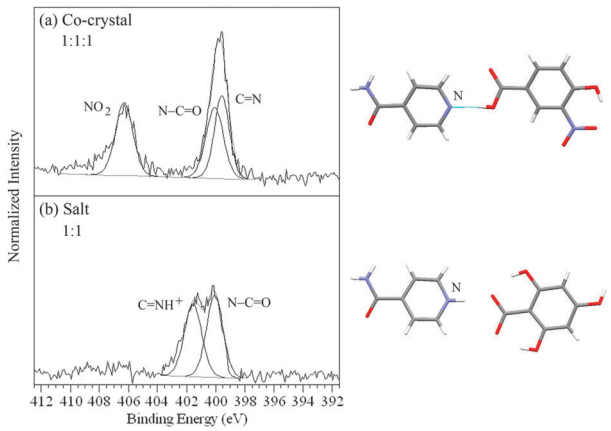

Fig. 4 N 1s XPS spectra of (a) the isonicotinamide/4-hydroxy-3-nitrobenzoic acid co-crystal and (b) the isonicotinamide/2,4,6-trihydroxybenzoic acid salt (NH_3^+, COO^-), with the corresponding intermolecular H-bonding/protonation from the single crystal XRD structures.

acid as a co-crystal and isonicotinamide/2,4,6-trihydroxybenzoic acid as a salt (Fig. 4).

The API **1** provides a variety of nitrogen environments (Fig. 1), which can be grouped into pyridine derivatives (C=N × 3), amines (C–N × 2), and amides (N–C=O × 2). For the free base form (API **1**), the photoemission by the C–N and C=N nitrogens appears around the same binding energy position at 399.1 ± 0.1 eV, while that of N–C=O ranges from 400.3 to 400.6 eV (Fig. 5, Table 2). Differences with respect to the free base are clearly evident for the salt **1s**, with the presence of a pyridinium C=NH^+ peak component at 401.2 eV shifted

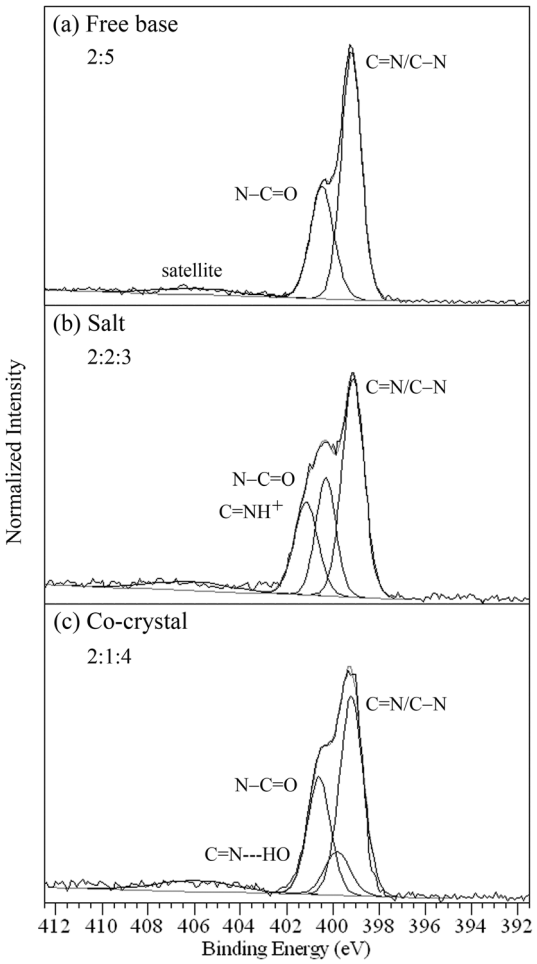

Fig. 5 N 1s XPS spectra of (a) the free base **1**, (b) di-HCl salt **1s**, and (c) fumaric acid co-crystal **1c** showing the ratios for the types of nitrogen.

by +2.1 eV compared to unprotonated, pyridine nitrogen (Fig. 5, Table 2). The relative intensity of this peak is in accord with the protonation of two of the pyridine nitrogens in the di-HCl salt **1s**. There is also an observable difference for the co-crystal **1c**, with a decrease in the intensity of the C–N/C=N peak relative to the free base and a broadening between the two free base peak components. This is accounted for by a third peak at 399.8 eV, of a relative intensity indicative of one of the C–N/C=N nitrogens (Fig. 5, Table 2). A shift of +0.6 eV from the C–N/C=N photoemissions is too small a magnitude for complete proton transfer, so it appears likely that formation of a new hydrogen bond results in a high binding energy shift for the nitrogen acceptor atom.

The difumarate salt **2** has three nitrogen environments (Fig. 1), comprising two heterocyclic amines (C–N × 2) and one sulfonamide (N–SO_2 × 1). The sulfonamide nitrogen gives rise to the peak at 399.5 eV, while protonation of the amine nitrogens results in a peak at 401.7 eV (Fig. 6a, Table 2), although this API is particularly sensitive to X-ray induced reduction of NH_3^+ to NH_2 (occurring at coinciding binding energy with N–SO_2), leading to a departure from the expected 2 : 1 ratio.[58] The HCl salts **3** and **4** have two and three nitrogens respectively

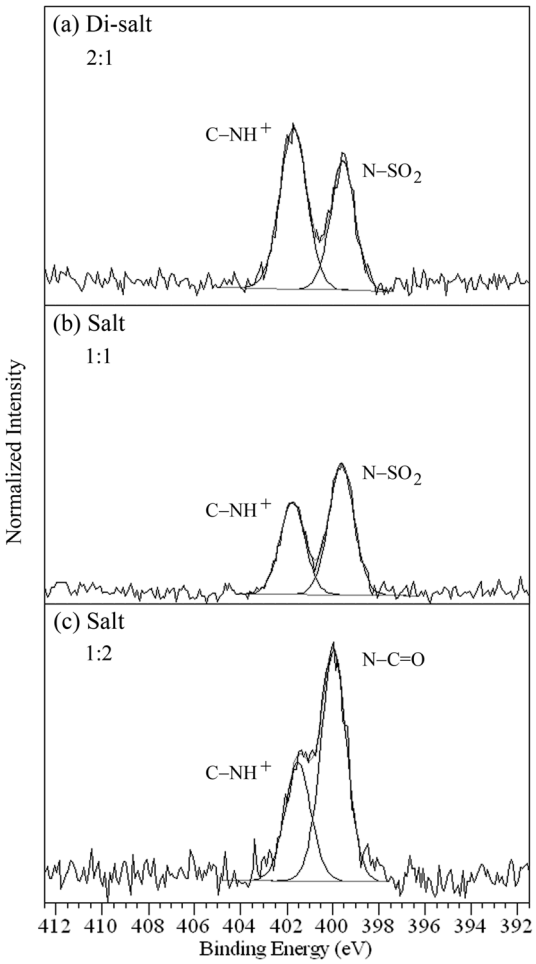

Fig. 6 N 1s photoemission of (a) difumarate salt **2**,[58] (b) HCl salt **3**, and (c) HCl salt **4** showing the ratios for the types of nitrogen.

(Fig. 1), with **3** including an amine (C–N × 1) and sulfonamide (N–SO_2 × 1), while **4** has a heterocyclic amine (C–N × 1) and two amides (N–C=O × 2). The sulfonamide peak of **3** and amide peak of **4** occur at 399.6 and 399.9 eV, respectively, while the protonated amine C–NH^+ nitrogen photoemissions occur at higher binding energy, 401.7 and 401.5 eV, respectively (Fig. 6b and c, Table 2).

^{15}N ssNMR

The spectra of the theophylline complexes,[21,28,30] **1s**, and **1c**, were compared with the free base form of each in order to investigate the changes in chemical shifts occurring with formation of the complexes. 50–100 ppm shifts relative to the starting components (chemical shift difference $\Delta\delta$) are typical for protonation of aromatic, heterocyclic nitrogen,[5,28–31] and shifts of 47–118 ppm to low frequency confirm salt formation (protonated nitrogen, C=NH^+) for the two theophylline/5-sulfosalicylic acid salts[28,30] (Table 3), the isonicotinamide/2,4,6-trihydroxybenzoic acid salt (Fig. 7, Table 5) and the di-HCl salt **1s** (Table 4). The theophylline salts are protonated at C=N (N9, Fig. 1, Table 3), with *ca.* −50 ppm shifts ($\Delta\delta$),[28,30] and the isonicotinamide salt has a −68.76 ppm shift on protonation (Fig. 7, Table 5), while di-HCl salt **1s** is protonated in two pyridine positions, N5 and N7, with shifts of −108.0 and −117.8 ppm respectively (Table 4). In contrast, the fumaric acid co-crystal **1c** (Table 4) and the theophylline co-crystal resonances[21,30] (Table 3) show only minor changes in ^{15}N chemical shifts compared to the base component ($\Delta\delta$), with the exception of the pyridine N5 resonance in **1c**. A shift of 32.6 ppm to low frequency occurs for N5 of **1c** (Table 4), indicating formation of a strong hydrogen bond that is not present in the free base form. A component of this change in chemical shift may be ascribed to conformational/crystallographic packing differences induced by the hydrogen bonding, which is observed on comparing different polymorphic forms of the free base.

Aliphatic nitrogen often exhibits much smaller shifts with protonation than its heterocyclic counterparts (*e.g.* amines *vs.* pyridines).[59] The aliphatic nature of the protonated nitrogen (C–NH_3^+) in the 3,5-diaminobenzoic acid/3,5-dinitrobenzoic acid salt results in a smaller magnitude shift of −14.11 ppm relative to the unprotonated amine, but this is still sufficient to distinguish formation of a salt from a co-crystal. There are no significant shifts indicating protonation of the amine in the 4-aminobenzoic acid co-crystals (Table 5), confirming they are not salts.

Table 3 ^{15}N ssNMR chemical shifts for the theophylline co-crystals and salts

	δ/ppm			
Compound	N1 O=C–N–C=O	N3 N–C=O	N7 C–N	N9 C=N
Theophylline	−227.04	−269.41	−218.47	−162.74
	$\Delta\delta = \delta$ (complex) − δ (theophylline)			
Complex (base/acid)	N1 O=C–N–C=O	N3 N–C=O	N7 C–N	N9 C=N
Theophylline/5-sulfosalicylic acid dihydrate salt	−0.60	−1.11	−2.44	−47.59
Theophylline/5-sulfosalicylic acid monohydrate salt	−1.34	−0.41	−5.33	−50.48
Theophylline/oxalic co-crystal	−0.44	1.99	−3.79	−1.82
Theophylline/maleic co-crystal	−0.81	1.96	−4.89	−5.39
Theophylline/malonic co-crystal	−3.85	3.31	−6.08	−4.07
Theophylline/citric co-crystal	−2.32	3.96	−8.16	3.72
Theophylline/glutaric co-crystal	−2.53	2.95	−4.16	1.01

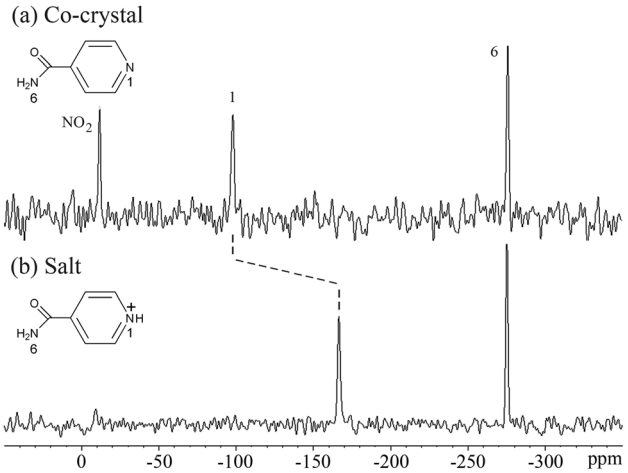

Fig. 7 ^{15}N ssNMR spectra of (a) the isonicotinamide/4-hydroxy-3-nitrobenzoic acid co-crystal and (b) the isonicotinamide/2,4,6-trihydroxybenzoic acid salt, showing the shift with proton transfer.

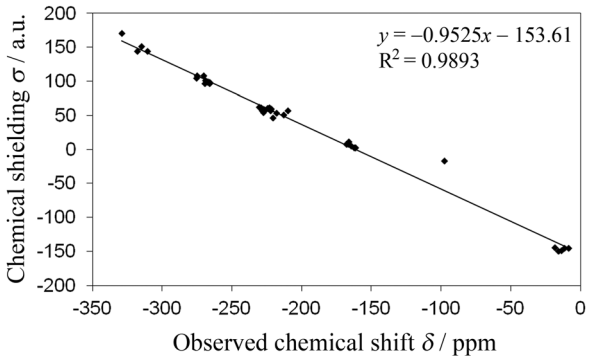

Fig. 8 CASTEP DFT nitrogen chemical shieldings (σ) *vs.* experimental ^{15}N ssNMR chemical shifts (δ).

Density functional theory (DFT) calculations (chemical shielding values, σ) were performed for the nitrogens of the theophylline, aminobenzoic, and isonicotinamide complexes in order to compare with experimental data (chemical shifts, δ). The plot of σ *versus* δ (Fig. 8) shows a linear correlation with $y = -0.9525x - 153.61$ ($R^2 = 0.9893$). This demonstrates the robustness of using CASTEP for relating ^{15}N ssNMR chemical shifts to molecular structure and, therefore, providing NMR based evidence for proof of co-crystal or salt formation.

The predicted chemical shift differences can be related to the H-bond length, giving a measure of H-bond strength, and providing an example of how NMR crystallography can be used in a complementary way with respect to X-ray crystallography.[60] For example, the predicted values as a function of distance between N of the base and H of the acid component show a clear separation between unprotonated (co-crystals, $d \geq 1.53$ Å) and protonated nitrogen (salts, $d \leq 1.11$ Å) for the theophylline complexes (Fig. 9). Additional multi-dimensional solid-state NMR studies are in progress to further characterize the nature of the hydrogen bonding in these co-crystals and salts.

ΔpK_a correlations

Plotting the nitrogen XPS and ssNMR values for the co-crystals and salts against ΔpK_a (Fig. 10) shows the dependence of the extent of proton transfer on the strength of the acidic component. Of the 17 complexes, the co-crystals have $\Delta pK_a \leq 0.3$, and the salts have $\Delta pK_a \geq 1.8$, with ΔpK_a ranging from −3.9 to 17.7, and four salts and two co-crystals have been assigned that are within the range for ΔpK_a typically viewed as the transition region (0–3) for which formation of a salt *vs.* co-crystal is not predictable.[12] Recently, pK_a matching has been used as a tool for predicting H-bond strengths[61] (including the proposed pK_a

Table 4 ^{15}N ssNMR chemical shifts for the salt (**1s**) and co-crystal (**1c**) of API **1**

	δ/ppm						
Compound	N1 amine	N2 amide	N3 amine	N4 amide	N5 pyridine	N6 pyridine	N7 pyridine
Free base (API **1**)	−298.04	−275.91	−249.82	−240.45	−93.20	−117.03	−70.04
	$\Delta\delta = \delta$ (complex) − δ (free base)						
Complex (base/acid)	N1 amine	N2 amide	N3 amine	N4 amide	N5 pyridine	N6 pyridine	N7 pyridine
Free base form I	0.91	−2.31	−0.58	1.93	−13.95	2.49	−4.30
Fumaric acid co-crystal **1c**	9.57	2.96	3.83	2.14	−32.60	2.82	1.12
Di-HCl salt **1s**	15.83	0.37	4.21	2.24	−108.02	−3.13	−117.79

Table 5 ^{15}N ssNMR chemical shifts for the aminobenzoic and isonicotinamide co-crystals and salts

	δ/ppm					
Complex (base/acid)	C=N	C–N	N–C=O	C=NH$^+$	C–NH$^+$	NO$_2$
4-Aminobenzoic acid/3,5-dinitrobenzoic acid co-crystal		−311.04				−16.28
4-Aminobenzoic acid/4-hydroxy-3-nitrobenzoic acid co-crystal		−318.15				−8.64
3,5-Diaminobenzoic acid/3,5-dinitrobenzoic acid salt		−314.94			−329.05	−14.13
						−18.53
Isonicotinamide/4-hydroxy-3-nitrobenzoic acid co-crystal	−97.87		−275.69			−11.61
Isonicotinamide/2,4,6-trihydroxybenzoic acid salt			−275.31	−166.63		

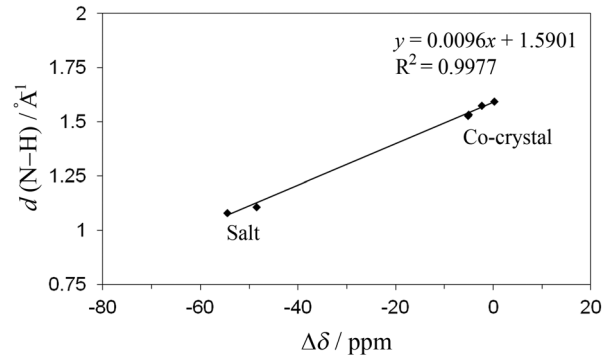

Fig. 9 CASTEP DFT optimised H-bond lengths *versus* predicted chemical shift differences ($\Delta\delta$).

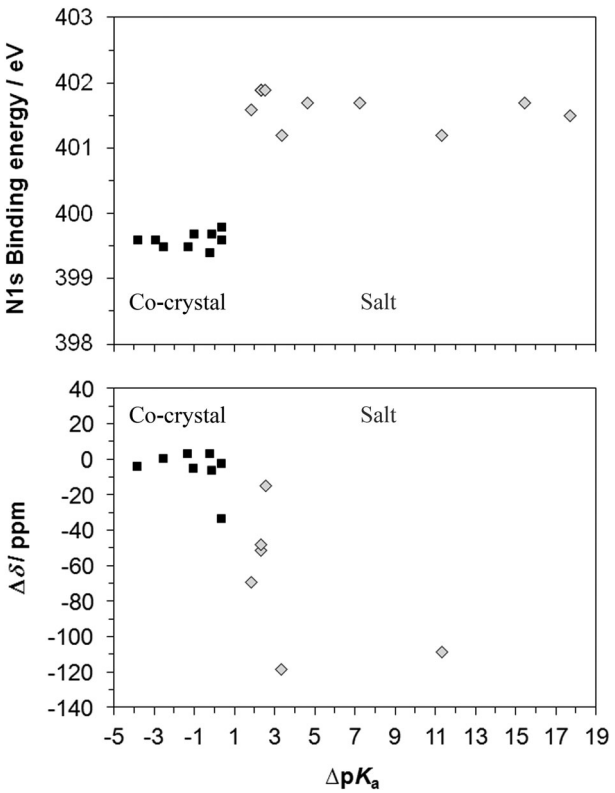

Fig. 10 Correlations between N 1s XPS and ^{15}N ssNMR chemical shifts with ΔpK_a, illustrating the clear separation between protonated (salt) and unprotonated nitrogen (co-crystal) with XPS and the overlap for new H-bond formation in a co-crystal (**1c**) and protonation of aliphatic nitrogen in a salt (3,5-diamino/3,5-dinitro) with ssNMR.

slide rule[62]). A correlation between bond lengths in crystals and ΔpK_a values was shown for N–H···O/O–H···N bonds.[62] In line with this work, we find a clear separation between N 1s XPS chemical shifts of the co-crystals around 399.6 eV and salts around 401.7 eV (Fig. 10). Measurement of the N 1s binding energy unambiguously determines whether protonation has occurred, with a mean N 1s binding energy difference of +2.1 eV for N → NH^+.

As the ^{15}N ssNMR chemical shift δ varies significantly with each base moiety and thus the absolute value is not a unique identifier for protonation state, the chemical shift difference ($\Delta\delta$, Fig. 10) is used to compare against the ΔpK_a for the complexes (no ssNMR data for API **2**, **3**, and **4**). There is a clustering of $\Delta\delta$ values for the co-crystals, although there is an overlap between co-crystals and salts. The smallest chemical shift observed for protonation of nitrogen (−14.11 ppm) and salt formation occurs for 3,5-diaminobenzoic acid/3,5-dinitrobenzoic acid and is a result of the reduced magnitude of the shift for aliphatic rather than heterocyclic aromatic nitrogen[59] as mentioned previously, and the theophylline and isonicotinamide salts exhibit $\Delta\delta$ of −50 to 70 ppm while the di-salt API **1s** shows larger magnitude shifts of around 110 ppm. The largest (most negative) shift for nitrogen within the co-crystals occurs for the development drug co-crystal **1c**, causing it to be greater than that of the signal from the aliphatic salt – formation of a strong hydrogen bond that is not present in the free base form (API **1**) is intimated for co-crystal **1c**, influencing the chemical shift, as well as a possible contribution from conformational/crystallographic packing differences. Comparing shifts between compounds sharing a component (such as salts and co-crystals which share the same free base) rather than the whole series clearly identifies each form correctly (Fig. 7, Tables 3–5).

XPS core level chemical shifts reflect primarily the influence of the most immediate atomic neighbours on the electronic state of the photoexcited atom,[33,48,50,63] with the effect of strong local intermolecular interactions such as ionic and H-bonding dominating over the comparatively weaker van-der-Waals and dipole interactions. It is for this reason that the core level binding energies reported in Table 2 and Fig. 10 are so universally sensitive to local structure and thus protonation state. In contrast, NMR is far more dependent on the extended environment and interactions, which leads to greater variance in $\Delta\delta$ as an indicator of protonation, although it does provide spatial resolution (allowing structurally inequivalent atoms of the same type of functional group to be distinguished). The combination of XPS and ssNMR to identify when hydrogen transfer has occurred from acid to base component is therefore especially strong, making assignment of salt or co-crystal unambiguous.

Conclusions

Nitrogen XPS and ssNMR chemical shifts clearly separate protonated from unprotonated nitrogen for a wide range of different solid-state donor–acceptor systems, including five pharmaceutical drug substances. The nature of the intermolecular interaction between the acid–base components was correctly identified for the eight salts and nine co-crystals. Brønsted proton transfer to nitrogen of the base component (salt formation) leads to chemical shifts towards higher core level binding energies in XPS and to lower frequency in ssNMR, while the hydrogen-bonded co-crystals exhibited only minor shifts compared to the free base form, with the exception of one of the pharmaceutical co-crystals (**1c**). The salt and co-crystal of the same API (**1**)

allowed comparison between the magnitude of the shift for formation of a strong hydrogen bond (at a position where there was none in the free base) compared to that for complete hydrogen transfer (protonation) at the same position in the salt. DFT-calculated ^{15}N ssNMR results show good correlation with experimental data, allowing prediction of chemical shifts and assignment of salt or co-crystal, and the strong influence of H-bond strength on the chemical shift.

Our data demonstrate both the versatility and unambiguity of such a combined XPS/ssNMR approach, which has, to our knowledge, never been systematically pursued before across such a large body of samples. The results will inform a more critical assessment of the possibilities and limitations associated with XPS and ssNMR, and provide a reference database for future investigations of hydrogen-bonding and protonation in other systems, for example the study of solvation effects in the nucleation and growth of organic crystals.[64]

Acknowledgements

We thank EPSRC and Sanofi-Aventis for previous financial support for JSS through a DTA/CTA studentship, and the EPSRC for the PhD + fellowship for JSS. We gratefully acknowledge support for SLMS, JSS, GS, and RJD through an ESPRC Critical Mass Grant (EP/1013563/1).

References

1 N. Schultheiss and A. Newman, *Cryst. Growth Des.*, 2009, **95**, 499–516.
2 P. Vishweshwar, J. A. McMahon, J. A. Bis and M. J. Zaworotko, *J. Pharm. Sci.*, 2006, **95**, 499–516.
3 C. B. Aakeroy, M. E. Fasulo and J. Desper, *Mol. Pharmaceutics*, 2007, **4**, 317–322.
4 *Handbook of Pharmaceutical Salts: Properties, Selection, and Use*, Wiley-VCH, Weinheim, 2002.
5 Z. J. Li, Y. Abramov, J. Bordner, J. Leonard, A. Medek and A. V. Trask, *J. Am. Chem. Soc.*, 2006, **128**, 8199–8210.
6 D. P. McNamara, S. L. Childs, J. Giordano, A. Iarriccio, J. Cassidy, M. S. Shet, R. Mannion, E. O'Donnell and A. Park, *Pharm. Res.*, 2006, **23**, 1888–1897.
7 A. V. Trask, W. D. S. Motherwell and W. Jones, *Int. J. Pharm.*, 2006, **320**, 114–123.
8 C. C. Sun and H. Hou, *Cryst. Growth Des.*, 2008, **8**, 1575–1579.
9 M. Viertelhaus, R. Hilfiker, F. Blatter and M. Neuburger, *Cryst. Growth Des.*, 2009, **9**, 2220–2228.
10 S. Chattoraj, L. Shi and C. C. Sun, *CrystEngComm*, 2010, **12**, 2466–2472.
11 C. M. Reddy, G. R. Krishna and S. Ghosh, *CrystEngComm*, 2010, **12**, 2296–2314.
12 S. L. Childs, G. P. Stahly and A. Park, *Mol. Pharmaceutics*, 2007, **4**, 323–338.
13 C. B. Aakeroy, A. Rajbanshi, Z. J. Li and J. Desper, *CrystEngComm*, 2010, **12**, 4231–4239.
14 M. Byres, P. J. Cox, G. Kay and E. Nixon, *CrystEngComm*, 2009, **11**, 135–142.
15 D. M. S. Martins, D. S. Middlemiss, C. R. Pulham, C. C. Wilson, M. T. Weller, P. F. Henry, N. Shankland, K. Shankland, W. G. Marshall, R. M. Ibberson, K. Knight, S. Moggach, M. Brunelli and C. A. Morrison, *J. Am. Chem. Soc.*, 2009, **131**, 3884–3893.
16 S. Mohamed, D. A. Tocher, M. Vickers, P. G. Karamertzanis and S. L. Price, *Cryst. Growth Des.*, 2009, **9**, 2881–2889.
17 A. Parkin, S. M. Harte, A. E. Goeta and C. C. Wilson, *New J. Chem.*, 2004, **28**, 718–721.
18 C. Wilson, *Crystallogr. Rev.*, 2007, **13**, 143–198.
19 R. Taylor and O. Kennard, *Acta Crystallogr., Sect. B: Struct. Sci.*, 1983, **39**, 133–138.
20 A. V. Trask and W. Jones, in *Organic Solid State Reactions*, ed. F. Toda, Springer-Verlag, New York, 2005, pp. 41–70.
21 J. S. Stevens, S. J. Byard and S. L. M. Schroeder, *Cryst. Growth Des.*, 2010, **10**, 1435–1442.
22 C. C. Wilson, K. Shankland and N. Shankland, *Z. Kristallogr.*, 2001, **216**, 303–306.
23 C. Wilson, *Acta Crystallogr., Sect. B: Struct. Sci.*, 2001, **57**, 435–439.
24 J. A. Cowan, J. A. K. Howard, G. J. McIntyre, S. M. F. Lo and I. D. Williams, *Acta Crystallogr., Sect. B: Struct. Sci.*, 2003, **59**, 794–801.
25 T. Steiner, I. Majerz and C. C. Wilson, *Angew. Chem., Int. Ed.*, 2001, **40**, 2651–2654.
26 C. C. Wilson, N. Shankland and A. J. Florence, *Chem. Phys. Lett.*, 1996, **253**, 103–107.
27 C. C. Wilson, N. Shankland and A. J. Florence, *J. Chem. Soc., Faraday Trans.*, 1996, **92**, 5051–5057.
28 J. S. Stevens, S. J. Byard, C. A. Muryn and S. L. M. Schroeder, *J. Phys. Chem. B*, 2010, **114**, 13961–13969.
29 R. Gobetto, C. Nervi, E. Valfre, M. R. Chierotti, D. Braga, L. Maini, F. Grepioni, R. K. Harris and P. Y. Ghi, *Chem. Mater.*, 2005, **17**, 1457–1466.
30 J. S. Stevens, S. J. Byard and S. L. M. Schroeder, *J. Pharm. Sci.*, 2010, **99**, 4453–4457.
31 T. Friščić, L. Fábián, J. C. Burley, D. G. Reid, M. J. Duer and W. Jones, *Chem. Commun.*, 2008, 1644–1646.
32 R. Gobetto, C. Nervi, M. R. Chierotti, D. Braga, L. Maini, F. Grepioni, R. K. Harris and P. Hodgkinson, *Chem.–Eur. J.*, 2005, **11**, 7461–7471.
33 J. S. Stevens, S. J. Byard, C. C. Seaton, G. Sadiq, R. J. Davey and S. L. M. Schroeder, *Angew. Chem., Int. Ed.*, 2011, **50**, 9916–9918.
34 P. A. Williams, C. E. Hughes, G. K. Lim, B. M. Kariuki and K. D. M. Harris, *Cryst. Growth Des.*, 2012, **12**, 3104–3113.
35 F. Bisti, A. Stroppa, S. Picozzi, M. Donarelli, S. Picozzi and M. Coreno, *J. Chem. Phys.*, 2013, **138**, 014308.
36 J. S. Stevens and S. L. M. Schroeder, *Surf. Interface Anal.*, 2009, **41**, 453–462.
37 G. Gilli and P. Gilli, *The Nature of the Hydrogen Bond*, Oxford University Press, Oxford, 2009.
38 *Experimental* pK_a values were obtained using the ACD/I-Lab Web service (ACD/pK_a DB 12.0), Advanced Chemistry Development, Inc. (ACD/Labs), Toronto, 2010.

39 *Predicted pK_a* values were obtained using ACD/PhysChem Suite v12.0, Advanced Chemistry Development, Inc. (ACD/Labs), Toronto, 2010.
40 J. S. Stevens, S. J. Byard, C. C. Seaton, G. Sadiq, R. J. Davey and S. L. M. Schroeder, *Angew. Chem.*, 2011, **123**, 10090–10092.
41 J. Madarász, P. Bombicz, K. Jármi, M. Bán, G. Pokol and S. Gál, *J. Therm. Anal. Calorim.*, 2002, **69**, 281–290.
42 C. C. Seaton, K. Chadwick, G. Sadiq, K. Guo and R. J. Davey, *Cryst. Growth Des.*, 2009, **10**, 726–733.
43 K. Chadwick, G. Sadiq, R. J. Davey, C. C. Seaton, R. G. Pritchard and A. Parkin, *Cryst. Growth Des.*, 2009, **9**, 1278–1279.
44 *Avantium Crystal16® parallel crystallizer*, Avantium, Amsterdam.
45 G. M. Sheldrick, *Acta Crystallogr., Sect. A: Fundam. Crystallogr.*, 2008, **64**, 112–122.
46 A. Altomare, G. Cascarano, C. Giacovazzo, A. Guagliardi, M. C. Burla, G. Polidori and M. Camalli, *J. Appl. Crystallogr.*, 1994, **27**, 435–436.
47 N. Fairley and A. Carrick, *The Casa Cookbook – Part 1: Recipes for XPS Data Processing*, Acolyte Science, Knutsford, Cheshire, 2005.
48 D. Briggs, M. P. Seah and P. M. A. Sherwood, in *Practical Surface Analysis, Volume 1: Auger and X-ray Photoelectron Spectroscopy*, ed. D. Briggs and M. P. Seah, John Wiley & Sons, Chichester, 2nd edn, 1990.
49 D. Briggs and G. Beamson, *Anal. Chem.*, 2002, **64**, 1729–1736.
50 *The XPS of Polymers Database*, Surface Spectra Ltd., Manchester, 2000.
51 R. K. Harris, E. D. Becker, S. M. Cabral De Menezes, R. Goodfellow and P. Granger, *Pure Appl. Chem.*, 2001, **73**, 1795–1818.
52 R. K. Harris, E. D. Becker, S. M. Cabral De Menezes, P. Granger, R. E. Hoffman and K. W. Zilm, *Pure Appl. Chem.*, 2008, **80**, 59–84.
53 J. R. Yates, C. J. Pickard and F. Mauri, *Phys. Rev. B: Condens. Matter Mater. Phys.*, 2007, **76**, 024401.
54 M. D. Segall, P. L. D. Lindan, M. J. Probert, C. J. Pickard, P. J. Hasnip, S. J. Clark and M. C. Payne, *J. Phys.: Condens. Matter*, 2002, **14**, 2717–2743.
55 S. J. Clark, M. D. Segall, C. J. Pickard, P. J. Hasnip, M. I. J. Probert, K. Refson and M. C. Payne, *Z. Kristallogr.*, 2005, **220**, 567–570.
56 R. K. Harris, P. Hodgkinson, C. J. Pickard, J. R. Yates and V. Zorin, *Magn. Reson. Chem.*, 2007, **45**, S174–S186.
57 *Materials Studio version 4.4*, Accelrys, Inc., San Diego, 2010.
58 J. S. Stevens, S. J. Byard, E. Zlotnikov and S. L. M. Schroeder, *J. Pharm. Sci.*, 2010, **100**, 942–948.
59 C. G. Levy and R. L. Litcher, *Nitrogen-15 Nuclear Magnetic Resonance Spectroscopy*, Wiley, New York, 1979.
60 *NMR Crsytallography*, John Wiley & Sons Ltd, Chichester, 2009.
61 P. Gilli, L. Pretto and G. Gilli, *J. Mol. Struct.*, 2007, **844–845**, 328–339.
62 P. Gilli, L. Pretto, V. Bertolasi and G. Gilli, *Acc. Chem. Res.*, 2009, **42**, 33–44.
63 K. Siegbahn, *ESCA: Atomic, Molecular, and Solid State Structure Studied by Means of Electron Spectroscopy*, Almqvist & Wiksells, Uppsala, 1967.
64 R. J. Davey, S. L. M. Schroeder and J. H. ter Horst, *Angew. Chem., Int. Ed.*, 2013, **52**, 2166–2179.

